Graphical Abstract

3D-Nanoflowers of Rutile TiO_2 as Film Grown on Conducing and Non-conducting Glass Substrates for *In-Vitro* Biocompatibility Studies with Mouse MC3T3 Osteoblast and Human HS-5 Cells

Kyung-Hee Park, Marshal Dhayal

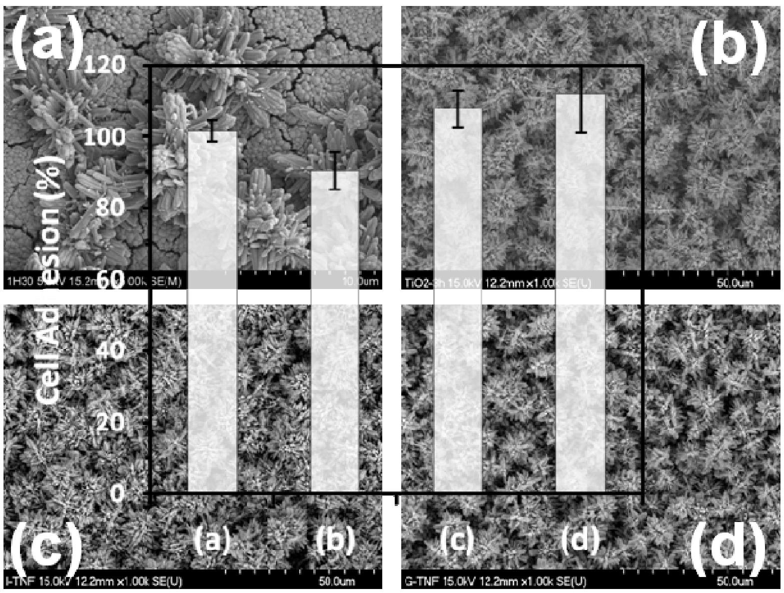

3D-Nanoflowers of Rutile TiO_2 as Film Grown on Conducting and Non-conducting Glass Substrates for *In-Vitro* Biocompatibility Studies with Mouse MC3T3 Osteoblast and Human HS-5 Cells

Kyung-Hee Park[a], *Marshal Dhayal*[b*]

[a]The Research Institute of Advanced Engineering Technology, Chosun University, Gwangju 501-759, Korea

[b]Clinical Research Facility, CSIR-Center for Cellular and Molecular Biology, Hyderabad 500007, Andhra Pradesh, India.

*Corresponding Author (Fax: +91 40 27160591; Tel: +91 40 27160222; E-mail address: marshal@ccmb.res)

Abstract

Thin films of 3D-nanoflowers of rutile TiO_2 on conducting (FTO and ITO) and non-conducting (glass) substrates were grown in a surfactant free one-step hydrothermal process. Field emission scanning electron microscope (FE-SEM) observations confirmed transformation of TiO_2 nanostructures from mesh like to 3D-nanoflowers with an increase in hydrolysis rate during the growth of TiO_2 films. X-ray diffraction (XRD) pattern of TiO_2 nanostructures as films grown on different substrates at various conditions had phase pure rutile crystallite structure. High resolution transmission electron microscopy (HR-TEM) diffraction pattern of the TiO_2 nanostructures showed tightly packed assemblies of titanium atoms and 0.23 nm lattice spacing along the longitudinal axis direction of rutile TiO_2. X-ray photoelectrons spectroscopic (XPS) analysis of TiO_2 nanostructures grown as films on glass substrates showed a spectra shift of 0.53 eV in binding energy which confirms the charge accumulation on non-conducting substrate whereas there was no spectral shift observed for TiO_2 films of similar structures grown on

conducting substrates. The accumulated charge on conducting surfaces can be easily neutralized whereas non-conducting surfaces may retain these accumulated charges. Adhesion, viability and proliferation response of mouse osteoblast (MC3T3) and human stromal (HS-5) cells on 3D-nanoflower of TiO_2 as films grown on conducting and non-conducting substrates was assessed. Adhesion and proliferation of both the cells showed better response on non-conducting surfaces as compare to conducting surfaces despite of having similar crystallite structures and nanomorphology of TiO_2. Stromal cells had potential to prepare extra cellular matrix scaffolds for ex-vivo expansion/differentiation of stem cells [1,2]. Hence the current findings can be used to prepare 3D TiO_2 nanostructure supported cellular scaffolds for regenerative medicine in the future.

Keywords: One step process, 3D nano-structures, charge distribution, bio-active surface

1. INTRODUCTION

During the past two decades, substantial research work has been carried out to understand the correlation between different process parameters of various synthesis methods and their effects on tailoring structural and functional properties of metal and metal oxides [3-8]. In the past the use of metal oxides such as titanium dioxides with tunable nano-structural and chemical properties has been extensively explored for catalytic, energy and biomedical applications [9-13]. Different synthesis methods were employed to tailor structural and functional properties of metal oxides by manipulating processing conditions to have desired arrangements of nanocrystallites [13-18]. For each synthesis method detailed studies were carried out to understand the effects of processing parameters on modification of basic structure properties but still it's a challenge to obtain the material with higher degree of phase purity, tunable surface morphologies with desired surface chemical functionalities [19-21].

A number of researchers have addressed the challenges associated with tunable surface morphology and synthesis of micro/nanostructures of titanium oxides with highly oriented rod-like crystals [22-27]. The control over crystallite phase and morphologies were achieved either by surface treatment or metal ion doping [28-31]. Thin films of titanium oxides were deposited with controllable crystallite phases by choosing appropriate metal ion doping and were used for different applications [32,33]. Well ordered 1D TiO_2 as nanorods, nanowires, nanocorals, hierarchical microspheres and nanotubes were synthesized and extensive studies were performed to use these for energy and biosensor applications [23-26]. Previously biocompatibility of titanium oxides as thin film coatings deposited by plasma sputtering and dip coating were studied with different types of cells [9,12,28]. The simultaneous growth of 1D/3D nanorods/nanoflowers is advantageous for better adhesion at interface of these 1D/3D nanostructures [34]. However, the use of 1D and 3D nano-assembles of TiO_2 in biomedical field is not fully explored yet.

Here we report a surfactant free one-step hydrothermal process for growth of 1D/3D nano-morphologies of TiO_2 at various conditions. The simultaneous growth of 3D nanoflowers like structures on 1D nanorods provides better adhesion at interface of 1D/3D nanoroads. The other advantage of the method used in this study was to achieve uniform coatings on all sides of the substrates in a single step. Physicochemical properties of these nanostructures of TiO_2 grown on different substrates (non-conducting glass and FTO/ITO coated conducting glass) were investigated. The effects of molar ratio of precursor material and reaction time were optimized to grow 1D/3D nanostructures of rutile TiO_2 as films on different types of substrates. In this study, first time we have reported cellular response of osteoblast and HS-5 cells with TiO_2 without alteration in 3D nano-structures by changing conducting and non-conducting nature of the substrates. The use of osteoblast cell for assessing the biocompatibility of metal oxide and polymeric materials is a well accepted *in-vitro* model system [35-38]. To further assess the usefulness of 1D/3D nanostructures, human stromal cells which has potential for preparing extra cellular matrix scaffold were cultured on different types of nanoassemblies of TiO_2. *In-vitro* cell adhesion, viability and proliferation asses with human HS-5 cells were performed. The outcomes of this study may have potential in future to use these substrates to prepare 3D nano-structures supported cellular scaffolds for application in regenerative medicine.

2. EXPERIMENTAL

2.1 Materials

Titanium isopropoxide ($Ti[OCH(CH_3)_2]_4$, 97%), hydrochloric acid (HCl, 37 wt%), and isopropyl alcohol were purchased from Sigma-Aldrich (Sigma-Aldrich) and used as received. The plastic wares used for cell culture in this study were from Nunc, USA. Culture media (α-MEM) was obtained from Invitrogen. All other tissue culture reagents and MTT (3-(4,5-Dimethylthiazol-2-yl)-2,5-diphenyltetrazolium were purchased from Sigma. All other analytical grade chemicals and solvents purchased from local companies.

2.2 Hydrothermal growth of TiO_2 nanostructures as films

For the growth of nanostructures of TiO_2 as films titanium isopropoxide solution was prepared in HCl. Six different dilution ratio of HCl with water as (**i**) 20:80, (**ii**) 30:70, (**iii**) 40:60, (**iv**) 50:50, (**v**) 60:40 and (**vi**) 70:30 were prepared and used to control the hydrolysis rate of titanium isoproposide. In the final step, 1ml of titanium isopropoxide was added to 40 ml of HCl solutions described above (of (**i**)-(**vi**)). Titanium isopropoxide mixed HCl solutions were placed in a teflon-lined stainless steel autoclave. The temperature of the autoclave was set at 180°C and the growth of nanostructures achieved at 3 h on FTO substrates for the conditions (**i**) to (**vi**). After the reaction was completed, the autoclave was allowed to cool to room temperature and the TiO_2 nanostructures grown on FTO substrates at different conditions as described above were collected and then dried in vacuum at 70^{o}C for 12h before use.

Fig. 1 shows FE-SEM images of nanostructures of TiO_2 grown on FTO at various dilution conditions of HCl ((**i**)-(**vi**)). TiO_2 nanostructures obtained at conditions ((**i**)-(**iii**)) having higher water content in HCl showed round ball like 3D TiO_2 nanostructures (**Fig. 1 a**,**b**&**c**). A very significant change in the surface structure morphology was observed with an increase in dilution of HCl. FE-SEM images of TiO_2 nanostructures obtained at higher concentration of HCl (at condition **vi**) shows mesh like nanostructure. Mesh like nanostructures of TiO_2 were changed to 3D-nanoflower like structure for the use of equal volume to volume ratio of water and HCl. TiO_2 nanostructures obtained at equal volume to volume ratio of water and HCl (condition **iv**) showed uniform distribution of 3D-nanoflowers of TiO_2 on FTO. Hence, this optimum condition (**iv**) was used for further investigation of the effects of time on TiO_2 nanostructure growth as films on FTO. In this study, three different types of substrates (i) non-conducting glass (glass), (ii) ITO coated conducting glass (ITO) and (iii) FTO coated conducting glass (FTO) were used.

The TiO_2 films grown at these four different types of conditions as (a) 1 h on FTO, (b) 3 h on FTO, (c) 3 h on ITO and (d) 3 h on glass substrates were used for quantification of detailed crystallite structure by X-ray diffraction (XRD), surface chemical analysis by X-ray photoelectron spectroscopy (XPS) and cell cultures experiments to assess the biocompatibility.

2.3 Cell Culture

The MC3T3 and HS-5 cells were maintained in α-MEM with 10% Fetal Bovine Serum (FBS) and 100 U/mL penicillin and incubated at 37 °C in an atmosphere of 5% CO_2. Trypsin-EDTA was used to detach the cells. Three samples were used for *in-vitro* cell adhesion, viability and proliferation assay and all the experiments were repeated for three times. For statistical analysis pair wise comparison of inter-experiment variation was done. MS Excel software was used for statistical analysis. Standard deviation values were calculated separately for all assays. The significance of the statistical analysis values was determined using Student's t-test where the p values of < 0.05 were considered significant. The cell culture experiments were performed on TiO_2 3D-nanoflower structures grown on FTO, ITO and glass substrates at the condition (**iv**) for 3 h. Additionally TiO_2 nanostructures grown at early stage (1h) on FTO substrate for condition (**iv**) was selected to perform cell culture experiments and tissue culture plastic surface were used as control condition.

2.4 Characterizations

The crystallite structure of TiO_2 1D and 3D nanostructures grown on different substrates was characterized from XRD pattern obtained by using a XRD-6000 (Japan) X-ray diffractometer in the diffraction angle range 5–80° with Cu-Kα radiation (λ= 1.54060 Å). Transmission electron microscopy (TEM) and high-resolution transmission electron microscopy (HRTEM) were performed using JEM 2010F microscope. TEM, selected area electron diffraction (SAED) patterns and HRTEM images were obtained by TECNAI F20 Philips operated at 200 kV. The surface morphology of the samples was recorded by a field emission scanning electron microscope (FESEM; S-4700, Hitachi). XPS spectra were obtained on a MultiLab200 with standard MgKα radiation to quantify elemental composition and surface states of TiO_2 nanostructures. All spectra were taken at a working pressure of 10^{-9} mbar. An XPS survey and high-resolution spectra of the C1s, O1s, and Ti2p were collected. The different surface states were obtained in the high resolution Ti2p, O1s and C1s spectra of the samples by specifying a line shape, relative sensitivity factor (RSF), peak position, full width at half maxima (FWHM), and area constraints.

2.5 In-vitro Assays

Cell adhesion and viability assays: These assays were performed by plating 3×10^4 cells on nanostructures surfaces of 1 cm^2 placed in tissue culture grade plates. After 4 h, non adherent cells were washed off and 100 μL of 2 mg/mL MTT was added to the remaining cells of each condition followed incubation at 37 °C and 5% CO_2 for 4 h**.** After removing culture medial, the reaction was stopped by adding dimethylsulfoxide and read at 595 nm in ELISA reader. In cell viability assay, after 24 h of incubation, MTT assay was performed as described above to calculate the percentage of cell viability.

Cell proliferation assay: The assay was performed by plating similar number of cells of all conditions in triplicates and incubated at three different time periods namely 24, 48 and 72 h. At each time periods cell number was calculated by MTT assay as described above.

3 RESULTS AND DISCUSSION

3.1 Surface Morphology and Crystallite Structure Characterization

Fig. 2 shows FE-SEM images of time dependent growth of TiO_2 nanostructure on FTO grown at 1 h and 3 h. The high resolution FE-SEM images of TiO_2 nanostructures grown at 1 h showed two distinct regions as 1D-nanorod and 3D-nanoflower nanostructures. The top view in FE-SEM image of the TiO_2 nanostructures surface morphologies grown at 3 h showed uniform coverage with 3D-nanoflowers. From these observations it appears that 1D-nanorods of TiO_2 grows on the substrates as films on which simultaneous growth of 3D-nanoflowers were initiated. Cross sections view of FE-SEM images of nanostructures obtained at 1h and 3h growth of TiO_2

demonstrates the formation of 3D-nanoflowers on vertically aligned 1D-nanorods of TiO_2. TiO_2 nanostructure surfaces obtained at 1 h of growth had both 1D-nanorodes and 3D-nanoflowers whereas at 3 h of the growth the surfaces were completely covered by 3D-nanoflowers.

The effect of different types of substrates on the growth of TiO_2 nanostructures as films was quantified by FE-SEM images of nanostructures grown on glass, ITO and FTO substrates at 3 h. A uniform distribution of 3D-nanoflowers of TiO_2 as films were seen for all three different types of substrates in FE-SEM images shown in **Fig. 3** (a,b &c). Higher resolution FE-SEM images of 3D nano-flower structures shows about 300-500 nm tips of nano-rode at the surface which were very tightly packed as shown in **Fig. 3** (d,e&f). Cross sectional FE-SEM image view showed formation of stable interface of 3D nano-flower like structures on these substrates.

TEM image of the tip of TiO_2 3D-nanoflowers on FTO substrates was obtained at different magnification and results are shown in **Fig. 4**. Presence of densely packed TiO_2 as nanorods was seen in TEM images. Diffraction pattern of TiO_2 was obtained and lattice spacing (d) of TiO_2 was calculated. The results showed d_{001} = 0.23 nm along the longitudinal axis direction pertains to the d-spacing of rutile TiO_2 (001) crystal planes.

Fig. 5 (A) shows XRD pattern of TiO_2 nanostructures grown on FTO substrates at 1 h and 3 h. FTO substrate shows several strong peaks of Sn at (110), (002), (112), (202) and (113) planes in XRD spectra (**Fig. 5** A(a)) as measured previously [39]. XRD pattern of FTO substrates and TiO_2 nano-structures as films grown on FTO at 1 h was similar. This may be due to smaller amount of TiO_2 growth, hence TiO_2 content was not detected by XRD in the presence of strong background of FTO substrate. TiO_2 nanostructures obtained at higher time points (at 3 h) showed TiO_2 XRD peaks appears at 2 theta values of 27.62, 36.28, 41.42, 44.16, 54.62, 56.72, 63.02, 69.28. These peaks were assigned (hkl) values (110), (101), (111), (210), (211), (220), (002) and

(301), respectively. All the diffraction peaks were marked to pure tetragonal rutile phase of TiO_2 (JCPDS no. 21–1276). XRD patterns of TiO_2 nanostructures grown on **FTO**, **ITO** and **glass** substrates are shown in **Fig. 5** B. The XRD peaks appear at 2 theta values of 27.62, 36.28, 41.42, 44.16, 54.62, 56.72, 63.02, 69.28. XRD pattern of TiO_2 nano-structures as films grown on threes three substrates at 3 h seem to be identical. These peaks were assigned (hkl) values (110), (101), (111), (210), (211), (220), (002) and (301), respectively.

3.2 Characterization of Surface Chemical Functionalities

XPS spectra of TiO_2 nanostructure surfaces were obtained at 1h and 3h on FTO for quantification of surface elemental analysis. The % proportions of oxygen (O) to titanium (Ti) atoms were obtained from wide scan XPS spectra and the results are shown in **Fig. 6**A. The O/Ti value was 3.1 for the TiO_2 nanostructure surfaces obtained at 1h which was reduced to 2.7 for the nanostructure obtained at 3 h. The reduction in O/Ti values at higher time may correspond to decrease in % proportion of oxygen atom at the surface. This observation also indicates that titania atoms are tightly packed at the surface which is also confirmed by FE-SEM and TEM observations.

High resolution Ti2p and O1s XPS spectra were shown in **Fig. 6** B & C. Details of peak fitting parameters for Ti2p and O1s are given in **Fig. 6** D [16]. A small increase in Ti^{4+} surface states of Ti2p was observed at the surface of TiO_2 obtained at 3h. The relative increase in the proportion of Ti2p surface states indicates relative decrease in number of oxygen atoms surrounding to Ti atoms in these nanostructure assemblies. Relative proportions of different oxidation states of oxygen in O1s XPS spectra at the surface of TiO_2 obtained after 1 h and 3 h and results are shown in **Fig. 6** (C). Oxygen atoms as O= (O^{2-}) surface states were increased with increasing the reaction time. These observations are consistent with the atomic % proportion obtained from wide scan XPS spectra.

XPS spectra of nanostructures grown as films on ITO, FTO and glass substrates were obtained to further quantify the chemical nature of nano-structures. The wide scan XPS spectra of TiO_2 on non-conducting (glass), conducting (ITO and FTO) substrates are shown in **Fig. 7**. Detailed elemental analysis and peak fitting for surface state quantification from C1s and Ti2p was done as described in our previous studies [27] and results are shown in **Fig 8** & **9**. The higher resolution C1s XPS spectra of TiO_2 film surface prepared on glass and ITO substrates was fitted with six peaks of different carbon environments as: hydrocarbon (C-H/C-C) at 284.6± 0.2 eV, (C-C(=O)OX) at 285± 0.1 eV, (C-OX) at 286.1± 0.2 eV, (C=O/O-C-O) at 287.6± 0.2eV, (C(=O)OX) at 289.2± 0.2 eV and C-Ti at 283± 0.2eV. TiO_2 film surface prepared on FTO coated glass substrates was fitted with five peaks of different carbon environments as: hydrocarbon (C-H/C-C) at 284.6± 0.2 eV, (C-C(=O)OX) at 285± 0.1 eV, (C-OX) at 286.1± 0.2 eV, (C=O/O-C-O) at 287.6± 0.2eV and (C(=O)OX) at 289.2± 0.2 eV. TiO_2 films on glass showed a spectra shift of 0.53 eV towards lower binding energy side which was adjusted to its original position. The bombardment of X-ray photons during XPS analysis causes a positive charge to accumulate at the non-conducting surface. This charge accumulation corresponds to 0.53 eV energy shift in the XPS spectra for the TiO_2 films grown on non-conducting substrates. There was no spectral shift observed for TiO_2 nano-structures grown on conducting (ITO and FTO) glass substrates.

Different titanium oxidation states were quantified in high resolution Ti2p XPS spectra of TiO_2 nanostructures grown on ITO, FTO and glass substrates. The spectra were fitted with four peaks as $Ti^{3+}2p_{3/2}$ at 453.2± 0.4 eV, $Ti^{4+}2p_{3/2}$ at 454.6± 0.2 eV, $Ti^{3+}2p_{1/2}$ at 455.8± 0.4 eV and $Ti^{4+}2p_{1/2}$ at 460.3± 0.2 eV. There was not much change in surface states of Ti2p obtained for TiO_2 nanostructures grown on glass and FTO substrates. TiO_2 nanostructures grown on ITO substrates showed significant increase in Ti^{3+} surface state of Ti2p.

A relative variation in the % proportion of the different surfaces states of C1s and Ti2p with different types of nano-structures film prepared on ITO, FTO and glass substrates are shown in **Fig. 10**. Mainly five different types of carbon surface states as C/C-H, C-C(=O)OX, C-OX, C=O and C(=O)OX were observed in TiO_2 films on all three substrates. Here we are interested to see the relative variation for three active functional groups C-OX, C=O and C(=O)OX present at the nano-surface obtained on ITO, FTO and glass substrates. The % proportion of hydroxyl functional group at the surface in TiO_2 nano-structures was significantly increased while the substrates were changed to glass, FTO and ITO, respectively for growth of TiO_2. There was no significant change in the % proportion of carbon atoms as C=O in C1s at the surface of TiO_2 nano-structures grown on different types of substrates. TiO_2 nano-structures grown on glass substrates showed highest level of carboxylic functional group. There was not much difference in % proportion of carboxylic functional of TiO_2 nanostructured surfaces on ITO and FTO substrates. An increase in the Ti^{3+} surface states of Ti2p was obtained from TiO_2 nanostructures grown on ITO substrates. There was not much different in Ti^{3+} surface states of Ti2p of TiO_2 nanostructures obtained on glass substrates and FTO coated conducting glass substrates.

3.3 Biocompatibility of TiO_2 nanostructures

Cell adhesion, viability and proliferation assays using MC3T3 osteoblast and HS-5 Cells were done on TiO_2 nanostructure surfaces obtained at 1h and 3h, respectively on FTO and the results are shown in **Fig. 11**. An increase in cell adhesion % on both types of nano-structures was obtained as compared to control condition (on tissue culture plastic surfaces). Combination of 1D-nanorode and 3D-nanoflower like structures of TiO_2 provide better entrapping of cells hence highest % of cell adhesion was obtained. The cell viability did not show significant variation on these two different types of nano-structures. The cell proliferation was also a little less on these as compared to the control condition. The HS-5 cell adhesion % was similar on both types of nanostructures of TiO_2. The HS-5 cells viability was increased on TiO_2 nanostructure of 1D-nanorode/3D-nanoflower as compared to control condition. However, the cell proliferation was reduced on these two types of nano-structures.

MC3T3 cell adhesion, viability and proliferation assays were done on TiO_2 nanostructures film grown on FTO, ITO and glass substrates and results are shown in **Fig. 12**. An overall increase in % cell adhesion on TiO_2 nano-structures grown on all three different types of substrates was observed as compare to tissue culture plastic surface. The highest % cell adhesion was obtained on 3D nano-flower structures of TiO_2 grown on glass surface. There was a relative decrease in % of cell adhesion on TiO_2 3D-nanoflowers grown on ITO and FTO, respectively as compared to the response observed on nano-structures on glass. A similar response was observed for % cell viability. Osteoblast cell proliferation on TiO_2 3D flowers grown on ITO and FTO was less as compared to control conditions despite of having higher % cell adhesion. XPS analysis of TiO_2 films on non-conducting glass substrates showed a spectra shift towards lower binding energy side. This observation indicates that TiO_2 films on non-conducting glass surface can retain the charge whereas TiO_2 films grown on conducting (ITO and FTO) substrates do not show charge accumulation. TiO_2 3D-nanoflowers grown on non-conducting glass substrate had showed higher cell proliferation rate as compared to the control conditions whereas decrease in cell proliferation was observed on TiO_2 3D flowers grown on ITO and FTO. Hence, the charge nature of substrate play an important role in determining cellular respond despite of similar nanostructure of same material.

HS-5 cell adhesion, viability and proliferation assays were done on TiO_2 nanostructures film grown on FTO, ITO and glass substrates and results are shown in **Fig. 13**. The HS-5 cell adhesion assay showed less % cell adhesion on TiO_2 nano-structures grown on FTO substrates as compare to nanostructures grown on ITO and glass substrates. TiO_2 nanostructures on non-conducting glass substrates showed highest % cell adhesion and proliferation for HS-5 cells.

Despite of similar nanostructure and crystallite structures of TiO_2 grown on conducting and non-conducting surfaces, the improved adhesion and proliferation response of both the cells on non-conducting surfaces confirms that the cells prefer non-conducting surfaces. This may enable these cells to create and sustain the local surface charge environment induced during cell-surface interactions for better cell growth on non-conducting surfaces which is not possible on the conducting surfaces.

4 CONCLUSIONS

Ordered growth of nanorod (1D) / nanoflower (3D) structures of TiO_2 was achieved on non-conducting and conducting (FTO and ITO coated) glass substrates. The method we have used was a surfactant free process for simultaneous growth of 1D/3D nanoroads and nanoflowers structure with better adhesion at the interface. TiO_2 nanostructures obtained at higher time points (at 3 h) on **FTO**, **ITO** and **glass** substrates are of rutile phase. The finding showed that mixed 1D-nanorode / 3D-nanoflower like structures showed better cell adhesion as compared to only 3D-nanoflower like structures. Cell viability and proliferation rate was higher on TiO_2 3D-nanoflower grown on non-conducting surface as compare to conducting substrates.

ACKNOWLEDGMENT

KHP thank that this research was supported by the Basic Science Research Program through the National Research Foundation of Korea (NRF), funded the Ministry of Science, ICT & Future Planning (2012R1A1A3010655). MD is thankful to Council of Scientific & Industrial Research (CSIR), India network project (Bioceramics) for financial support. We are thankful to Dr Vijay Kumar (NIMS, Hyderabad) for permitting to use ELISA reader.

References

(1) Tiwari, A.; Tursky, M.L.; Mushahary, D.; Wasnik, S.; Collier, F.M.; Suma, K.; Kirkland, M.A.; Pande, G. *Ex-vivo* expansion of haematopoietic stem/progenitor cells from human umbilical cord blood on acellular scaffolds prepared from MS-5 stromal cell line. *Journal of Tissue Engineering and Regenerative Medicine*, **2013**, 7(11), 871-883.

(2) Goerner, M.;, Roecklein, B.; Torok-Storb, B.; Heimfeld, S.; Kiem, H.P. Expansion and transduction of nonenriched human cord blood cells using HS-5 conditioned medium and FLT3-L. *J Hematother Stem Cell Res*., **2000**, 9(5), 759-765.

(3) Rao, C.N.R.; Cheetham, A.K. Science and technology of nanomaterials: current status and future prospects. *J. Mater. Chem*., **2001**, 11, 2887-2894.

(4) Aruna, S.T.; Mukasyan, A.S. Combustion synthesis and nanomaterials. *Current Opinion in Solid State and Materials Science*, **2008**, 12(3-4), 44-50.

(5) Yang, P.; Zhao, D.; Margolese, D.I.; Chmelka, B.F.; Stucky, G.D. Generalized syntheses of large-pore mesoporous metal oxides with semicrystalline frameworks. *Nature*, **1998**, 396, 152-155.

(6) Li , J.; Tang , S.; Lu, L.; Zeng, H.C. Preparation of Nanocomposites of Metals, Metal Oxides, and Carbon Nanotubes via Self-Assembly. *J. Am. Chem. Soc.*, **2007**, 129 (30), 9401-9409.

(7) Agrawal S.V.; Reddy, S.S.; Dhayal, M. Ultra small gold nanoparticles synthesis in aqueous solution and their application in fluorometric collagen estimation using bi-ligand functionalisation, *RSC Advances*, **2014**, 4(35), 18250-18256.

(8) Nalwa, H.S. *Encyclopedia of nanoscience and nanotechnology*, American Scientific Publisher: USA, 2011.

(9) Dhayal, M.; Kapoor, R.; Sistla, P.G.; Kant, C.; Pandey, R.R.; Govind; Saini, K.K.; Pande, G. Ni doped TiO_2 thin films on borosilicate glass enhance in-vitro growth and differentiation of osteoblasts. *Journal of Biomedical Materials Research Part A*, **2012**, 100A(5), 1168-1178.

(10) Maira, A.J.; Yeung, K.L.; Lee, C.Y.; Yue, P.L.; Chan, C.K. Size effects in gas-phase photo-oxidation of trichloroethylene using nanometer-sized TiO_2 catalysts. *J. Catal*, **2000**, 192, 185-196.

(11) Carbone, R.; Marangi, I.; Zanardi, A.; Giorgetti, L.A.; Chierici, E.; Berlanda, G.; Podesta, A.; Fiorentini, F.; Bongiorno, G.; Piseri, P.; Pelicci, P.G.; Milani, P. Biocompatibility of cluster-assembled nanostructured TiO_2 with primary and cancer cells. *Biomaterials*, **2006**, 27, 3221-3229.

(12) Dhayal, M.; Kapoor, R.; Sistla, P.G.; Pandey, R.R.; Kar, S.; Saini K.K.; Pande, G. Strategies to prepare TiO_2 thin films, doped with transition metal ions, that exhibit specific physicochemical properties to support osteoblast cell adhesion and proliferation. *Mat. Sci.Eng. C*, **2014**, 37, 99–107.

(13) Zhao, W.; Chen, C.; Ma, W.; Zhao, J.; Shuai, Z. Efficient degradation of toxic organic pollutants with $Ni_2O_3/TiO_{(2-x)}B_x$ under visible irradiation. *J. Am. Chem. Soc.,* **2004**, 126, 4782-4783.

(14) Mazaheri, M.; Zahedi, A.M.; Haghighatzadeh, M.; Sadrnezhaad, S.K. Sintering of titania nanoceramic: Densification and grain growth. *Ceramics International*, **2009**, 35, 685-691

(15) Dhayal, M.; Sharma, S.D.; Kant, C.; Saini, K.K.; Jain, S.C. Role of Ni doping in surface carbon removal and photo catalytic activity of nano-structured TiO_2 film. *Surface Science*, **2008**, 602, 1149-1154.

(16) Jun, J.; Shin, J.H.; Dhayal, M. Surface state of TiO_2 treated with low ion energy plasma. *Applied Surface Science*, **2005**, 252(10), 3871-3877.

(17) Shah, S.I.; Li, W.; Huang, C.P.; Jung, O.; Ni, C. Study of Nd^{3+}, Pd^{2+}, Pt^{4+}, and Fe^{3+} dopant effect on photoreactivity of TiO_2 nanoparticles. *Proceedings of the National Academy of Sciences*, **2002**, 99(2), 6482-6486.

(18) Cheng, Y.; Sun, H.; Jin, W.; Xu, N. Photocatalytic degradation of 4-chlorophenol with combustion synthesized TiO_2 under visible light irradiation. *J. Chem. Eng.*, **2007**, 128, 127-133.

(19). Ma, P.X. Biomimetic materials for tissue engineering. *Adv. Drug. Deliv. Rev.*, **2008**, 60, 184-198.

(20) Liu, X.; Ding, C. Plasma sprayed wollastonite/TiO_2 composite coatings on titanium alloys. *Biomaterials*, **2002**, 23, 4065-4077.

(21) Kommireddy, D.S.; Sriram, S.M.; Lvov, Y.M.; Mills, D.K. Stem cell attachment to layer-by-layer assembled TiO_2 nanoparticle thin films. *Biomaterials*, **2006**, 27, 4296-4303.

(22) Zhang, H.; Han Y.; Liu X.; Liu P.; Yu H.; Zhang S.; Yao X.; Zhao H. Anatase TiO_2 microspheres with exposed mirror-like plane {001} facets for high performance dye-sensitized solar cells (DSSCs). *Chem. Comm.*, **2010**, 46, 8395-8397.

(23) Pandey, R.R.; Saini, K.K.; Dhayal, M. Using Nano-arrayed structures in sol-gel derived Mn^{2+} doped TiO_2 for high sensitivity urea biosensor, *Journal of Biosensors and Bioelectronic*, **2010**, 1: 101.

(24) Li Y.; Sun Q.; Sun X.; Dong L. Synthesis of nanocoral structured TiO_2 and its photoelectrical performance in dye sensitized solar cells. *ECS Trans.* **2013**, 53, 57-63.

(25) Li L.L.; Chen Y.J.; Wu H.P.; Wang N.S.; Diau E.W.G. Detachment and transfer of ordered TiO_2 nanotube arrays for front-illuminated dye-sensitized solar cells. *Energ. Environ. Sci.* **2011**, 4, 3420-3425.

(26) Qu J.; Lai C. One-dimensional nanostructures as photoanodes for dye-sensitized solar cells. *J. Nanomater*. **2013**, 2013 Article ID 762730.

(27) Adachi M.; Murata Y.; Takao J.; Jiu J.; Sakamoto M.; Wang F. Highly efficient dye-densitized solar cells with a titania thin-film electrode composed of a network structure of single-crystal-like TiO_2 nanowires made by the "oriented attachment" mechanism. *J. Am. Chem. Soc*. **2004**, 126, 14943-14949.

(28) Dhayal, M.; Cho, S.I.; Moon, J.Y.; Cho, S.J.; Zykova, A. S180 cell growth on low ion energy plasma treated TiO_2 thin films. *Appl. Surf. Sci.*, **2008**, 254, 3331-3338.

(29) Pandiyaraj, K.N.; Selvarajan, V.; Pavese, M.; Falaras, P.; Tsoukleris, D. Investigation on surface properties of TiO_2 films modified by DC glow discharge plasma. *Curr. Appl. Phys.*, **2009**, 9, 1032-1037.

(30) Ichinose, I.; Senzu, H.; Kunitake, T. Stepwise adsorption of metal alkoxides on hydrolyzed surfaces: A surface sol–gel process. *Chem. Lett.*, **1996**, 25, 831-832.

(31) Boyan, B.D.; Hummert, T.W.; Dean, D.D.; Schwartz, Z. Role of material surfaces in regulating bone and cartilage cell response. *Biomaterials*, **1996**, 17, 137-146.

(32) Randey, R.R.; Dhayal, M.; Saini K.K. Engineering electrochemical response of TiO_2-based enzymatic biosensors by aliovalent cation doping. *Advanced Electrochemistry*, **2013**, 1(1), 62-66.

(33) Randey, R.R.; Dhayal, M.; Saini, K.K. Modification of titanium surface states by ruthenium to enhance electrochemical response of TiO_2 thin films for biosensor application. *Adv. Electrochem.*, **2013**, 1(2), 55-61.

(34) Park, K.H.; Dhayal, M. Simultaneous growth of rutile TiO_2 as 1D/3D nanorod/nanoflower on FTO in one-step process enhances electrochemical response of photoanode in DSSC. *Electrochemistry Communication*, **2014**, 49, 47-50.

(35) Vagaska, B.; Bacakova, L.; Filova, E.; Balik, K. *Physiol. Res.,* **2010**, 59, 309-322.

(36) Chen, W.H.; Tabata Y.; Tong, Y.W. *Curr. Pharm. Des.,* **2010**, 16, 2388-2394.

(37) Wilson, C.J.; Clegg, R.E.; Leavesley D.I.; Pearcy, M.J. *Tissue Eng. Part A,* **2005**, 11, 1-18.

(38) Trinadh, M.; Kannan, G.; Rajasekhar, T.; Sainath, A.V.S.; Dhayal, M. Synthesis of glycopolymers at various pendant spacer lengths of glucose moiety and their effects on adhesion, viability and proliferation of osteoblast cells. *RSC Advances*, **2014**, 4(70), 37400-37410.

(39) Park, K.H.; Pandey, R.R.; Hong, C.K.; Saini, K.K., Dhayal, M. Electrochemical characterization of enzymatic organo-metallic coating of TiO_2 nanoparticles. *Sensors and Actuators B*, **2014**, 196, 589-595.

Figure Captions

Figure 1: FE-SEM images of rutile TiO_2 nanostructures grown on FTO substrates. (a), (b), (c), (d), (e) and (f) represents nano-structures grown at different dilution of HCl. HCl to water ratio (a) 20:80; (b) 30:70; (c) 40:60; (d) 50:50; (e) 60:40; (f) 70:30 at 180^{o}C.

Figure 2: FE-SEM images of rutile TiO_2 nanostructures grown on FTO substrates at two different times (1 h and 3 h) for HCl to water ratio 50:50 at 180 ^{o}C.

Figure 3: FE-SEM images of rutile TiO_2 nanostructures grown on glass (a), FTO (b) and ITO (c) substrates at 50:50 dilution of HCl with water and reaction time at 3 h and 180 ^{o}C.

Figure 4: (A) FE-SEM image of TiO_2 nanostructures grown on FTO substrates at 50:50 volume to volume ratio of HCl with water and 180 ^{o}C for 3 h. TEM images (B & C) of the tip-view of TiO_2 nanostructures as seen in high resolution FE-SEM image (A). (D) Diffraction pattern of TiO_2 nanostructures grown at similar conditions.

Figure 5: (A) XRD pattern of TiO_2 crystallite growth on FTO at 50:50 volume to volume ratio of HCl with water and 180^{o}C for two different times (1 h and 3 h). Prominent diffraction peaks in the XRD pattern of FTO substrate are marked with '*'. (B) XRD pattern of TiO_2 crystallite

growth on glass (a), FTO (b) and ITO (c) substrates at 50:50 volume to volume ratio of HCl with water and 180 ^{o}C for 3 h.

Figure 6: Wide scan XPS spectra of TiO_2 nanostructure growth on FTO substrates at 50:50 volume to volume ratio of HCl with water and 180^{o}C for two different reaction times. of (a) 1 h and (b) 3h.

Figure 7: (A) high resolution peak fitted Ti2p XPS spectra and (C) high resolution peak fitted O1s XPS spectra of TiO_2 nanosurfaces prepared at 50:50 volume to volume ratio of HCl with water and 180^{o}C for two different reaction times. (B) peak fitting parameter for Ti2p high resolution XPS spectra and (D) peak fitting parameter for O1s high resolution XPS spectra. (a) and (b) represents 1 h and 3h of TiO_2 nanostructure growth on FTO substrates, respectively.

Figure 8: Wide scan XPS spectra of TiO_2 nanosurfaces prepared at 50:50 volume to volume ratio of HCl with water and 180 ^{o}C for 3 h of reaction time on glass (a), FTO (b) and ITO (c) substrates.

Figure 9: High resolution C1s peak fitted XPS spectra of TiO_2 nanosurfaces prepared at 50:50 volume to volume ratio of HCl with water and 180 ^{o}C for 3 h of reaction time on glass (a), FTO (b) and ITO (c) substrates.

Figure 10: High resolution Ti2p XPS spectra of TiO_2 nanosurfaces prepared at 50:50 volume to volume ratio of HCl with water and 180 ^oC for 3 h of reaction time on glass (a), FTO (b) and ITO (c) substrates.

Figure 11: Relative variation in the % proportion of (A) COX in C1s, (B) CO in C1s, (C) C(=O)OX in C1s and (D) Ti^{3+} in Ti2p XPS spectra of TiO_2 nanosurfaces prepared at 50:50 volume to volume ratio of HCl with water and 180 ^oC for 3 h of reaction time on glass (a), FTO (b) and ITO (c) substrates.

Figure 12: Cell adhesion assay done by using MTT on TiO_2 nanostructures grown at (a) 1 h and (b) 3 h on FTO substrates and (c) tissue culture plastic surfaces. (A) The percentage of osteoblast cell adhesion. The significance values between the groups were determined: ♦ represents $p < 0.05$ for conditions (a) and (b) with respect to condition (c); ◊ represents $p < 0.05$ for condition (a) with respect to condition (b). (B) The percentage of osteoblast cell viability. ♦ Represents $p < 0.05$ for condition (a) with respect to condition (c); ◊ represents $p < 0.05$ for condition (a) with respect to condition (b). (C) Osteoblast cell proliferation. ♦ Represents $p < 0.05$ for conditions (a), (b) and (c) at different times of cell proliferation. ◊ Represents $p < 0.05$ for condition (a) and condtions (b) with respect to conditions (c) at the same cell proliferation time points. (D) The percentage of HS-5 cell adhesion. ♦ Represents $p < 0.05$ for condition (a) and condition (b) with respect to condition (c); ◊ represents $p < 0.05$ for condition (a) with respect to condition (b). (E)

The percentage of HS-5 viability. ♦ Represents $p < 0.05$ for condition (a) with respect to condition (c); ◊ represents $p < 0.05$ for condition (a) with respect to condition (b). (F) HS-5 cell proliferation. ♦ Represents $p < 0.05$ for conditions (a), (b) and (c) at different cell proliferation times. ◊ Represents $p < 0.05$ for conditions (a) and (b) with respect to condition (c) at same cell proliferation time.

Figure 13: Osteoblast cell response were observed on (a) tissue culture plastic surfaces and 3D nanoflower like TiO_2 nanostructures grown on (b) FTO, (c) ITO and (d) glass substrates at 3 h. (A) adhesion %, the significance values between the groups were determined: ♦ represents $p < 0.05$ for conditions (b), (c) and (d) with respect to condition (a); ◊ represents $p < 0.05$ for condition (c) and (d) with respect to condition (b); ● represents $p < 0.05$ for condition (d) with respect to condition (c). (B) viability %, ♦ represents $p < 0.05$ for conditions (b), (c) and (d) with respect to condition (a); ◊ represents $p < 0.05$ for condition (c) and (d) with respect to condition (b); ● represents $p < 0.05$ for condition (d) with respect to condition (c). (C) Cell proliferation, ♦ Represents $p < 0.05$ for conditions (a), (b), (c) and (d) with respect to change in cell proliferation time. ◊ Represents $p < 0.05$ for conditions (b), (c) and (d) with respect to condition (a) at same cell proliferation time.

Figure 14: HS-5 cell response were observed on (a) tissue culture plastic surfaces and 3D nanoflower like TiO_2 nanostructures grown on (b) FTO, (c) ITO and (d) glass substrates at 3 h. (A) adhesion %, the significance values between the groups were determined: ♦ represents p <

0.05 for conditions (b), (c) and (d) with respect to condition (a); ◊ represents $p < 0.05$ for condition (c) and (d) with respect to condition (b); ● represents $p < 0.05$ for condition (d) with respect to condition (c). (B) viability %, ♦ represents $p < 0.05$ for conditions (b), (c) and (d) with respect to condition (a); ◊ represents $p < 0.05$ for conditions (c) and (d) with respect to condition (b); ● represents $p < 0.05$ for condition (d) with respect to condition (c). (C) Cell proliferation, ♦ Represents $p < 0.05$ for conditions (a), (b), (c) and (d) with respect to change in cell proliferation time. ◊ Represents $p < 0.05$ for conditions (b), (c) and (d) with respect to condtion (a) at same cell proliferation time.

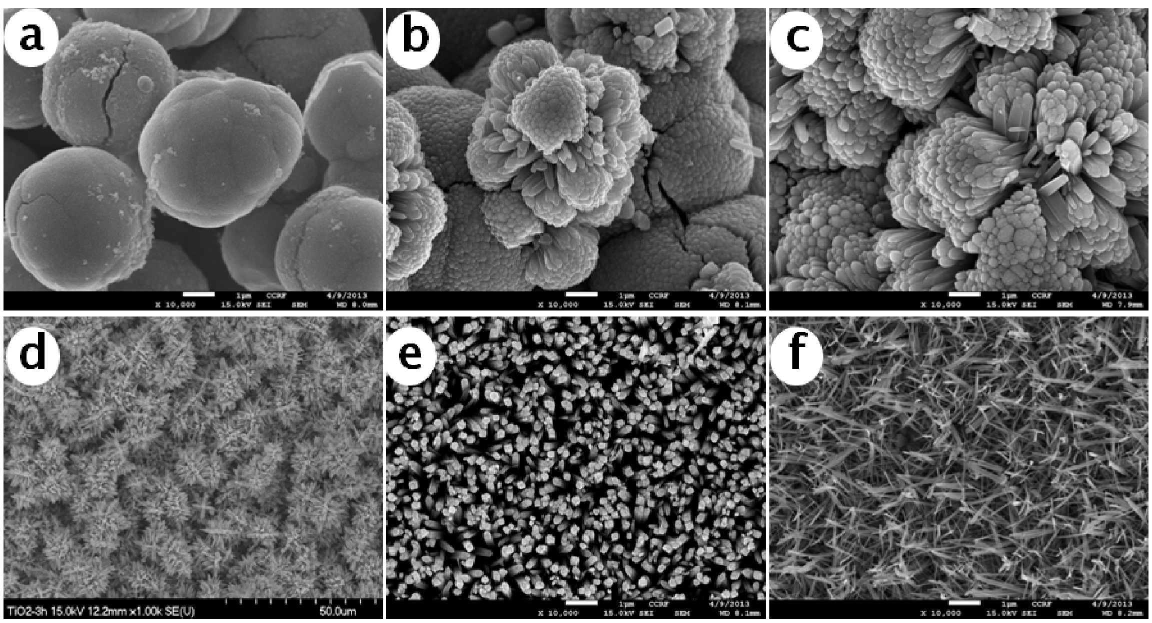

Figure 1

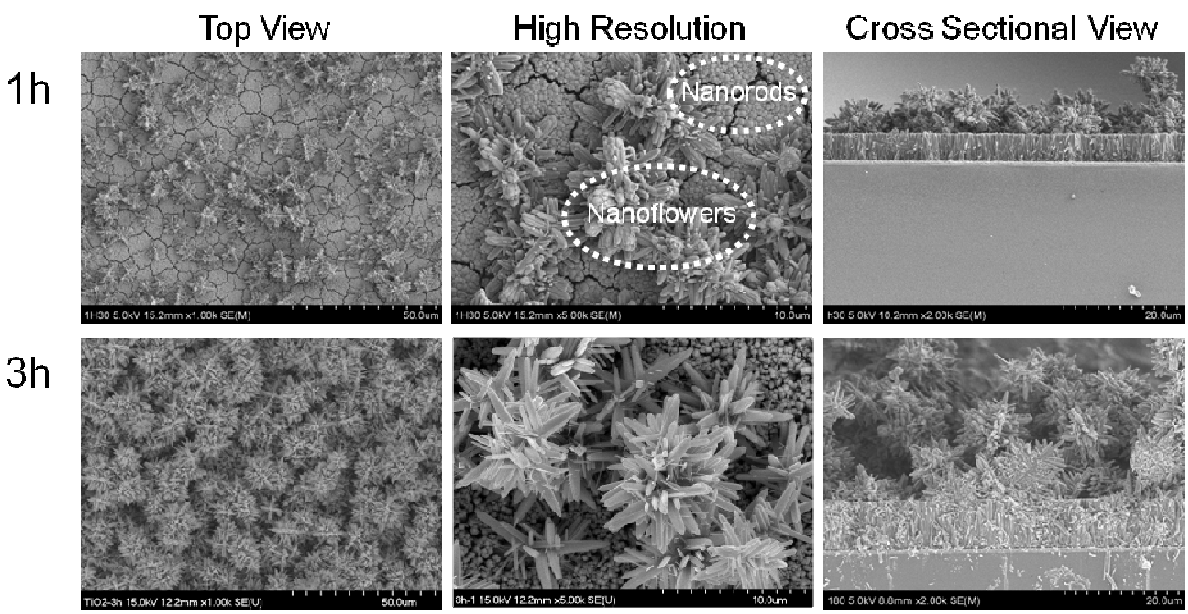
Top View
High Resolution
Cross Sectional View
1h
3h
Nanorods
Nanoflowers

Figure 2

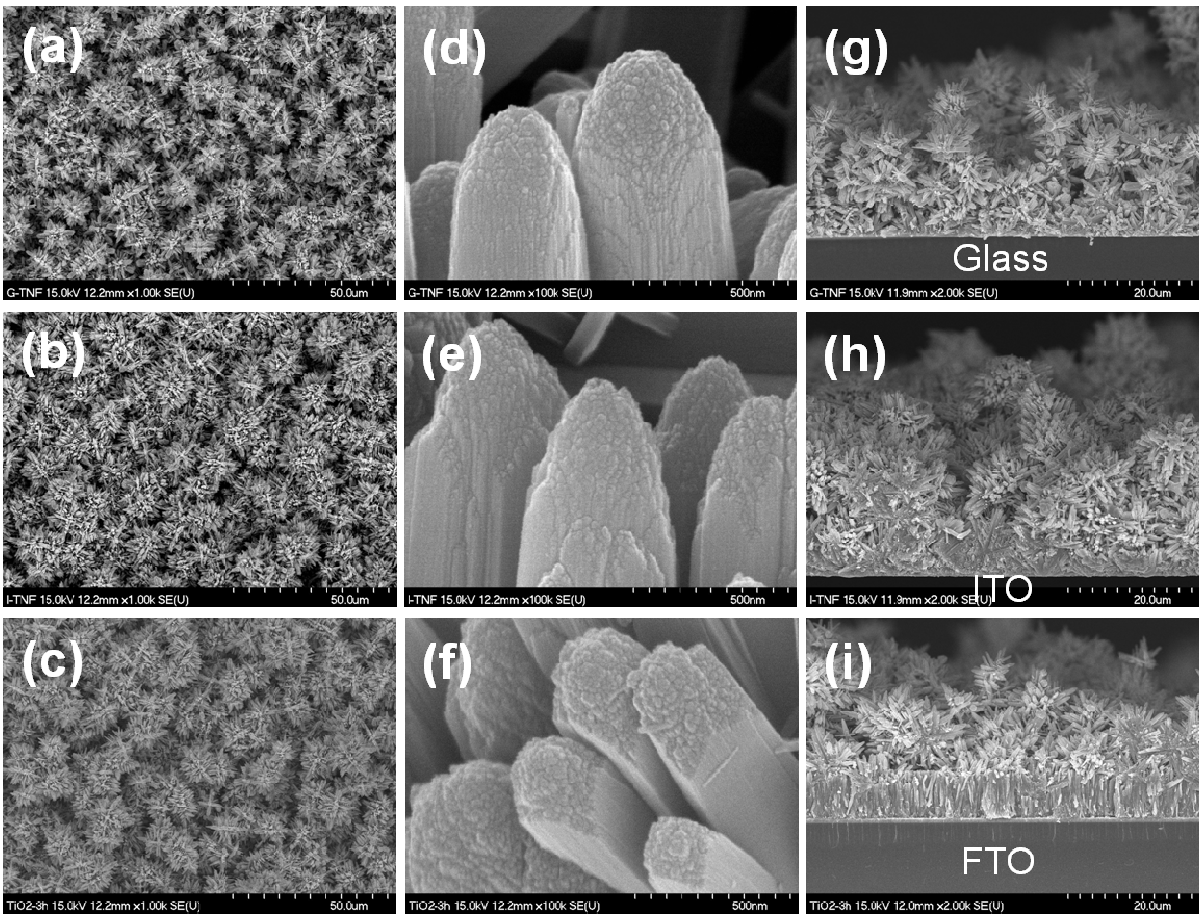
(a)
(d)
(g)
Glass
(b)
(e)
(h)
ITO
(c)
(f)
(i)
FTO
G-TNF 15.0kV 12.2mm x1.00k SE(U) 50.0um
G-TNF 15.0kV 12.2mm x100k SE(U) 500nm
G-TNF 15.0kV 11.9mm x2.00k SE(U) 20.0um
I-TNF 15.0kV 12.2mm x1.00k SE(U) 50.0um
I-TNF 15.0kV 12.2mm x100k SE(U) 500nm
I-TNF 15.0kV 11.9mm x2.00k SE(U) 20.0um
TiO2-3h 15.0kV 12.2mm x1.00k SE(U) 50.0um
TiO2-3h 15.0kV 12.2mm x100k SE(U) 500nm
TiO2-3h 15.0kV 12.0mm x2.00k SE(U) 20.0um

Figure 3

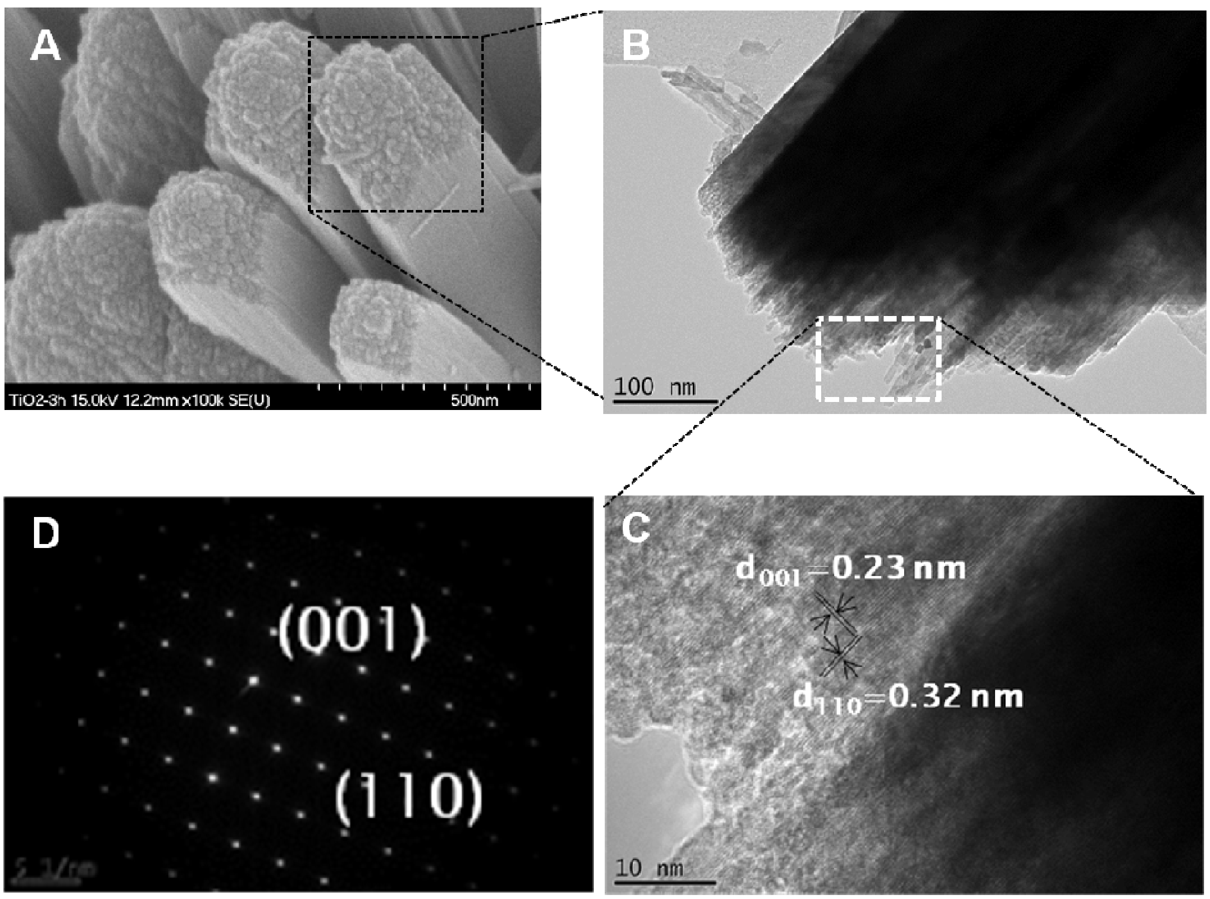
A
B
C
D
TiO2-3h 15.0kV 12.2mm x100k SE(U)
500nm
100 nm
10 nm
d_{001}=0.23 nm
d_{110}=0.32 nm
(001)
(110)

Figure 4

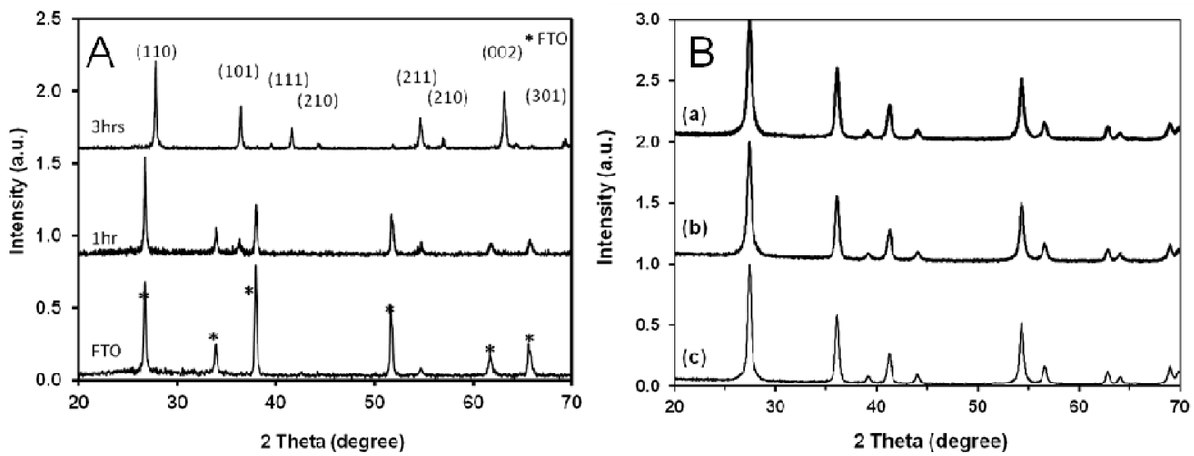
A
(110)
(101)
(111)
(210)
(211)
(210)
(002)
* FTO
(301)
3hrs
1hr
FTO
Intensity (a.u.)
2 Theta (degree)
B
(a)
(b)
(c)
Intensity (a.u.)
2 Theta (degree)

Figure 5

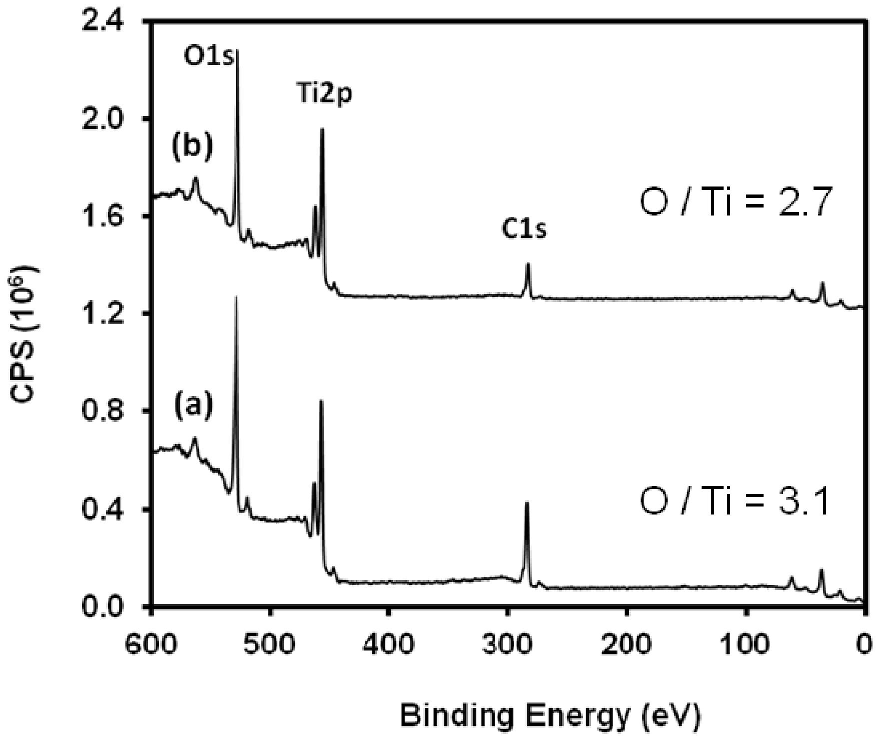
O1s
Ti2p
(b)
O / Ti = 2.7
C1s
(a)
O / Ti = 3.1
CPS (10^6)
2.4
2.0
1.6
1.2
0.8
0.4
0.0
600
500
400
300
200
100
0
Binding Energy (eV)

Figure 6

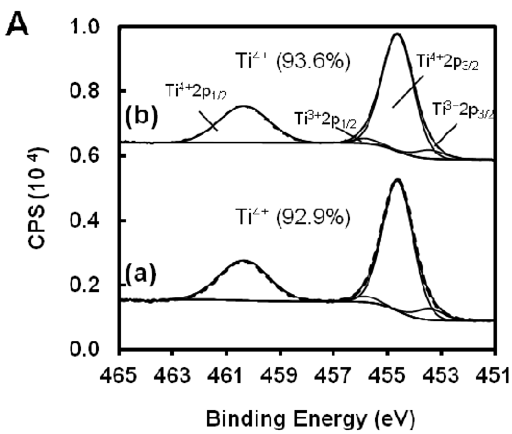

B

(a)

Environment	Position / eV	FWHM / eV	Ti / at %
Ti^{4+} $2p_{3/2}$	454.6	1.3	61.9
Ti^{4+} $2p_{1/2}$	460.3	2.1	31
Ti^{3+} $2p_{3/2}$	453.4	1.2	4.7
Ti^{3+} $2p_{1/2}$	455.8	1.1	2.4

(b)

Environment	Position / eV	FWHM / eV	Ti / at %
Ti^{4+} $2p_{3/2}$	454.6	1.4	62.4
Ti^{4+} $2p_{1/2}$	460.3	2.2	31.2
Ti^{3+} $2p_{3/2}$	453.4	1.2	4.3
Ti^{3+} $2p_{1/2}$	455.8	1.1	2.1

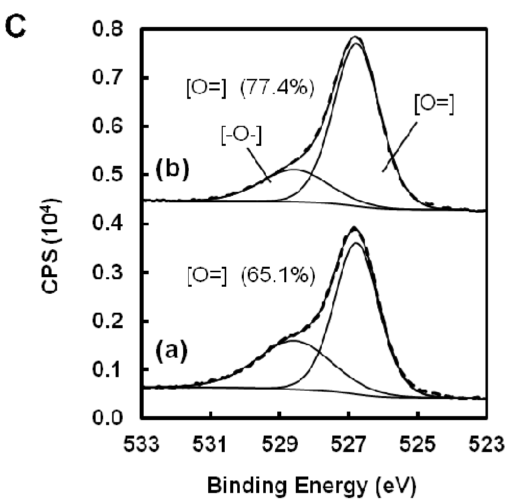

D

(a)

Environment	Position / eV	FWHM / eV	Oxygen / at %
[O=]	526.8	1.5	65.1
[-O-]	528.6	2.5	34.9

(b)

Environment	Position / eV	FWHM / eV	Oxygen / at %
[O=]	526.8	1.6	77.4
[-O-]	528.6	2.3	22.6

Figure 7

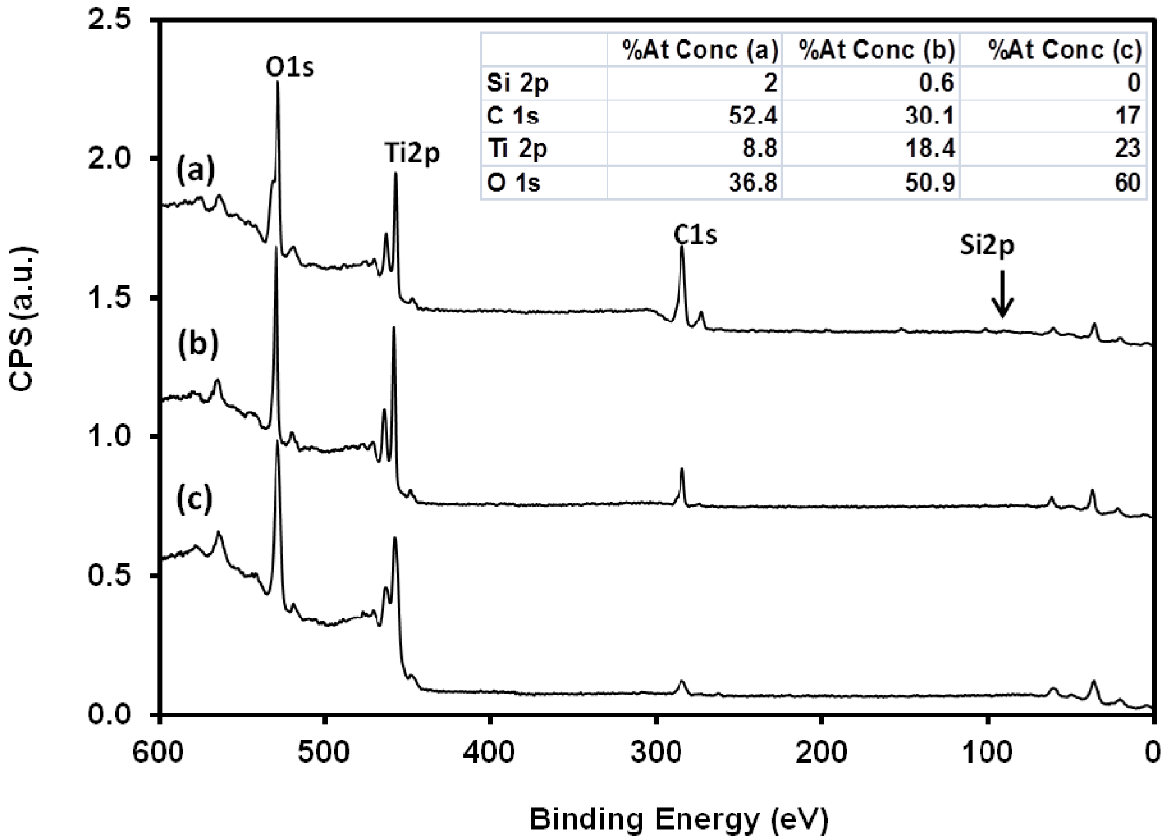
2.5
2.0
1.5
1.0
0.5
0.0
CPS (a.u.)
600
500
400
300
200
100
0
Binding Energy (eV)
O1s
Ti2p
C1s
Si2p
(a)
(b)
(c)
%At Conc (a) %At Conc (b) %At Conc (c)
Si 2p 2 0.6 0
C 1s 52.4 30.1 17
Ti 2p 8.8 18.4 23
O 1s 36.8 50.9 60

Figure 8

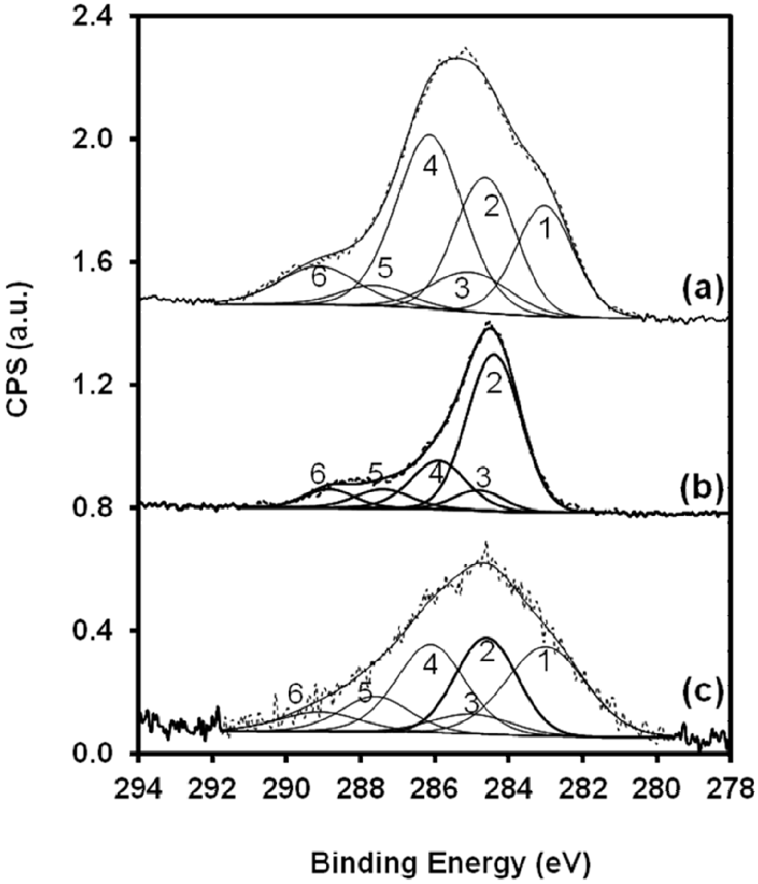

(a)	Position / eV	FWHM / eV
1	283	2.5
2	284.6	1.7
3	285	1.6
4	286.1	1.74
5	287.6	1.75
6	289.1	1.56

(b)	Position / eV	FWHM / eV
2	284.6	1.7
3	285	1.6
4	286.1	1.74
5	287.6	1.75
6	289.1	1.56

(c)	Position / eV	FWHM / eV
1	283	2.5
2	284.6	1.7
3	285	1.6
4	286.1	1.74
5	287.6	1.75
6	289.1	1.56

Figure 9

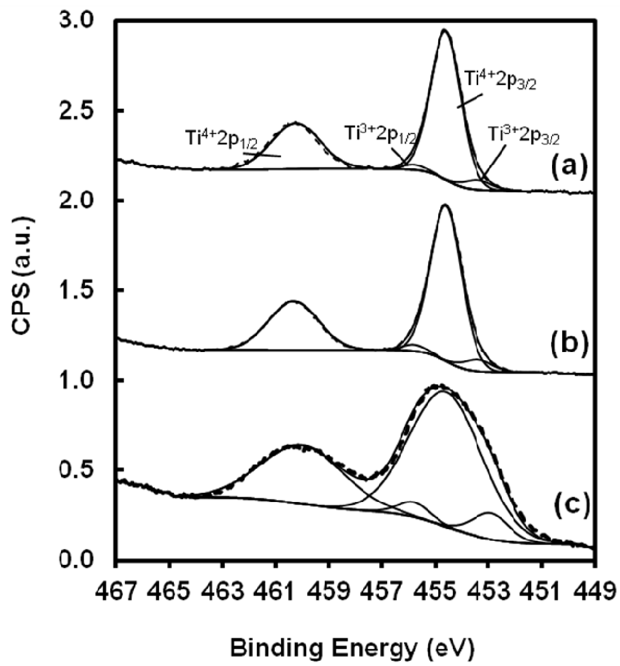

(a)

Environment	Position / eV	FWHM / eV	Ti / at %
Ti^{4+} $2p_{3/2}$	454.6	1.33	62.9
Ti^{4+} $2p_{1/2}$	460.3	2.1	31.4
Ti^{3+} $2p_{3/2}$	453.4	1.2	4.8
Ti^{3+} $2p_{1/2}$	455.8	1.1	1.9

(b)

Environment	Position / eV	FWHM / eV	Ti / at %
Ti^{4+} $2p_{3/2}$	454.6	1.4	62.4
Ti^{4+} $2p_{1/2}$	460.3	2.2	31.2
Ti^{3+} $2p_{3/2}$	453.4	1.2	4.3
Ti^{3+} $2p_{1/2}$	455.8	1.1	2.1

(c)

Environment	Position / eV	FWHM / eV	Ti / at %
Ti^{4+} $2p_{3/2}$	454.6	3.2	60.7
Ti^{4+} $2p_{1/2}$	460	3.65	30.3
Ti^{3+} $2p_{3/2}$	452.9	1.6	6
Ti^{3+} $2p_{1/2}$	455.8	1.4	3

Figure 10

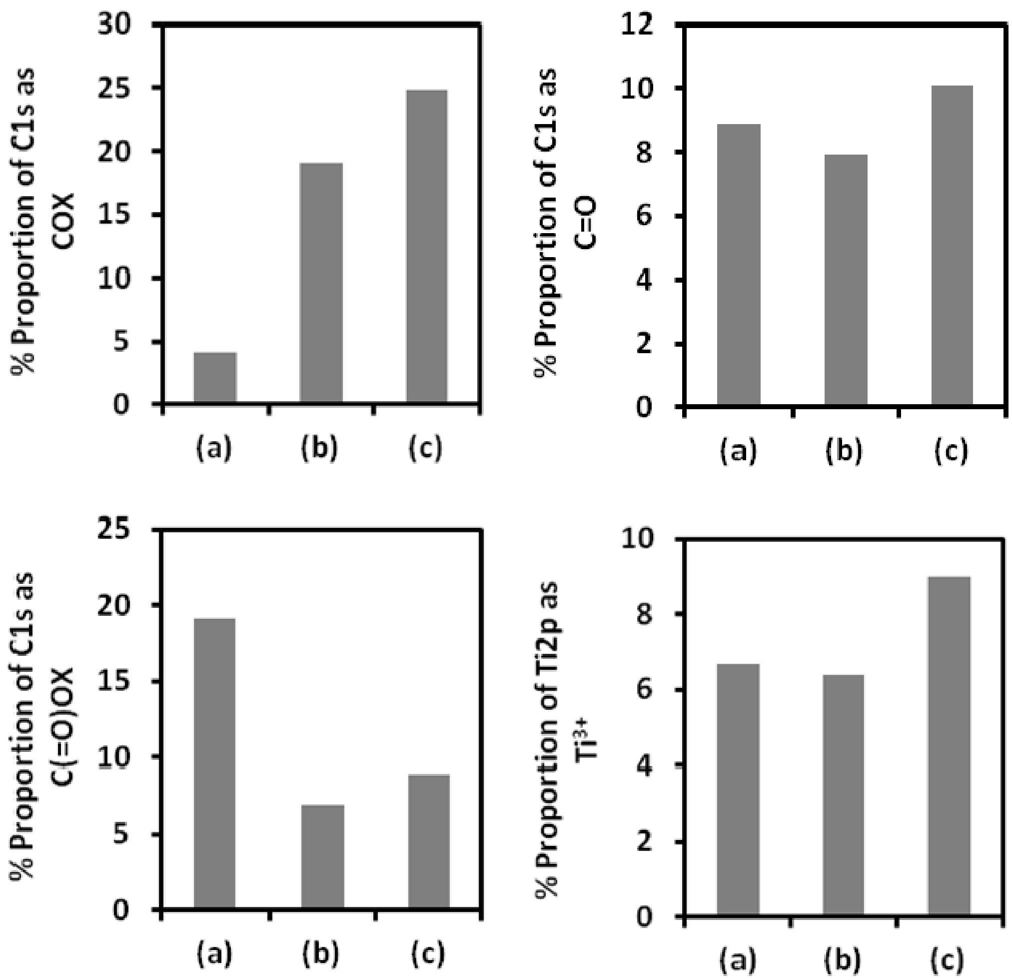
30
25
20
15
10
5
0
% Proportion of C1s as COX
(a)
(b)
(c)
12
10
8
6
4
2
0
% Proportion of C1s as C=O
(a)
(b)
(c)
25
20
15
10
5
0
% Proportion of C1s as C(=O)OX
(a)
(b)
(c)
10
8
6
4
2
0
% Proportion of Ti2p as Ti3+
(a)
(b)
(c)

Figure 11

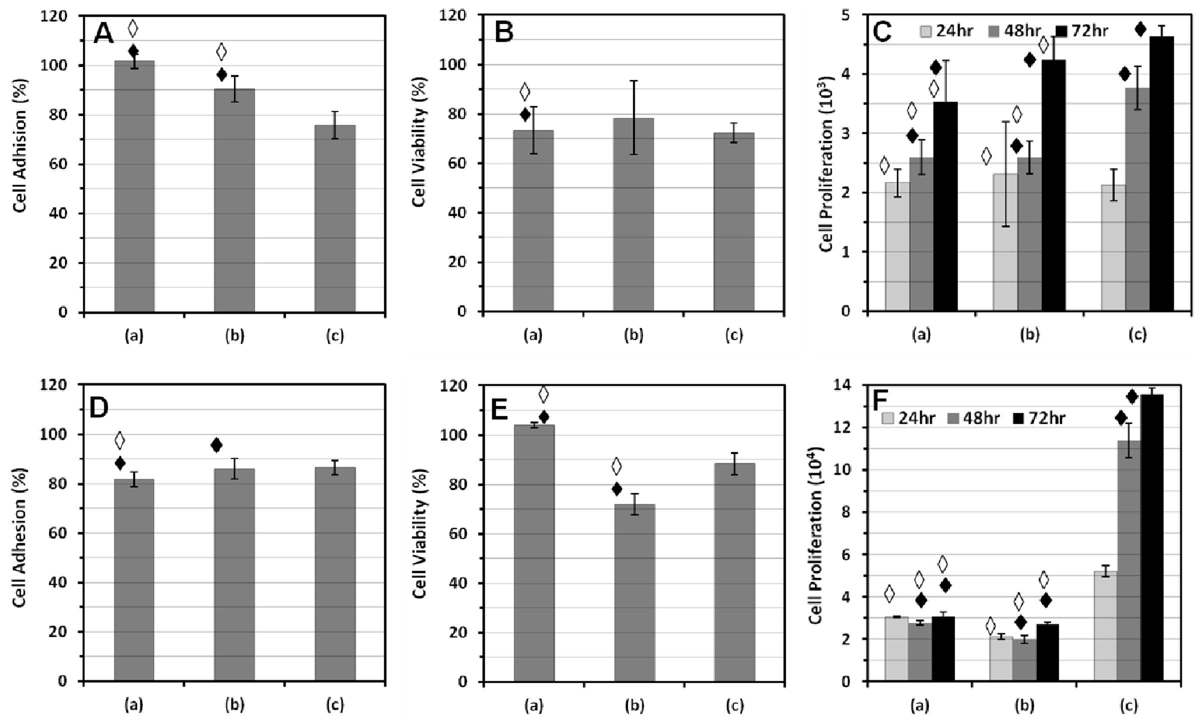
A
B
C
D
E
F
Cell Adhision (%)
Cell Viability (%)
Cell Proliferation (10^3)
Cell Adhesion (%)
Cell Proliferation (10^4)
24hr
48hr
72hr
(a)
(b)
(c)

Figure 12

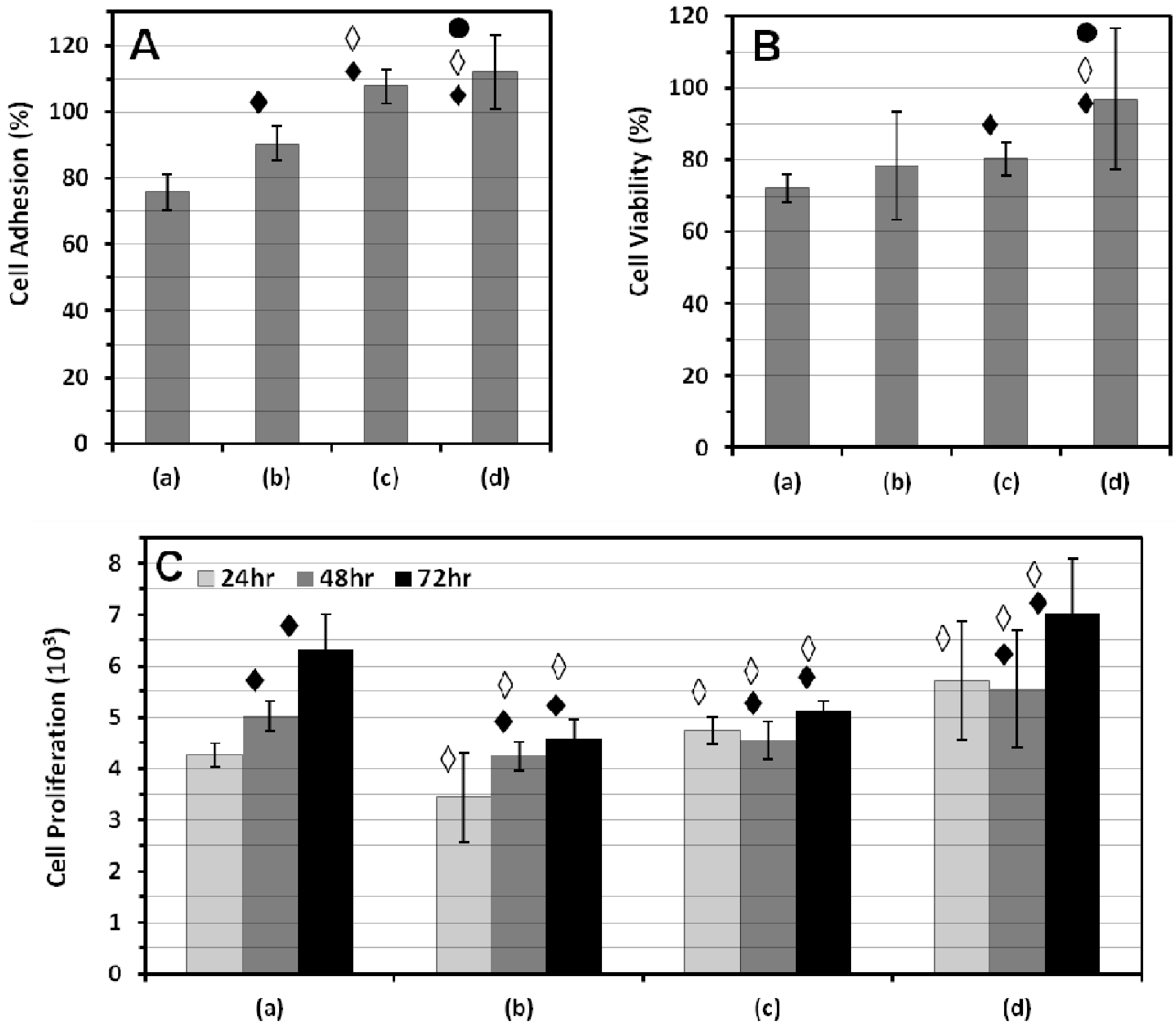
A
Cell Adhesion (%)
0
20
40
60
80
100
120
(a)
(b)
(c)
(d)
B
Cell Viability (%)
0
20
40
60
80
100
120
(a)
(b)
(c)
(d)
C
24hr
48hr
72hr
Cell Proliferation (10^3)
0
1
2
3
4
5
6
7
8
(a)
(b)
(c)
(d)

Figure 13

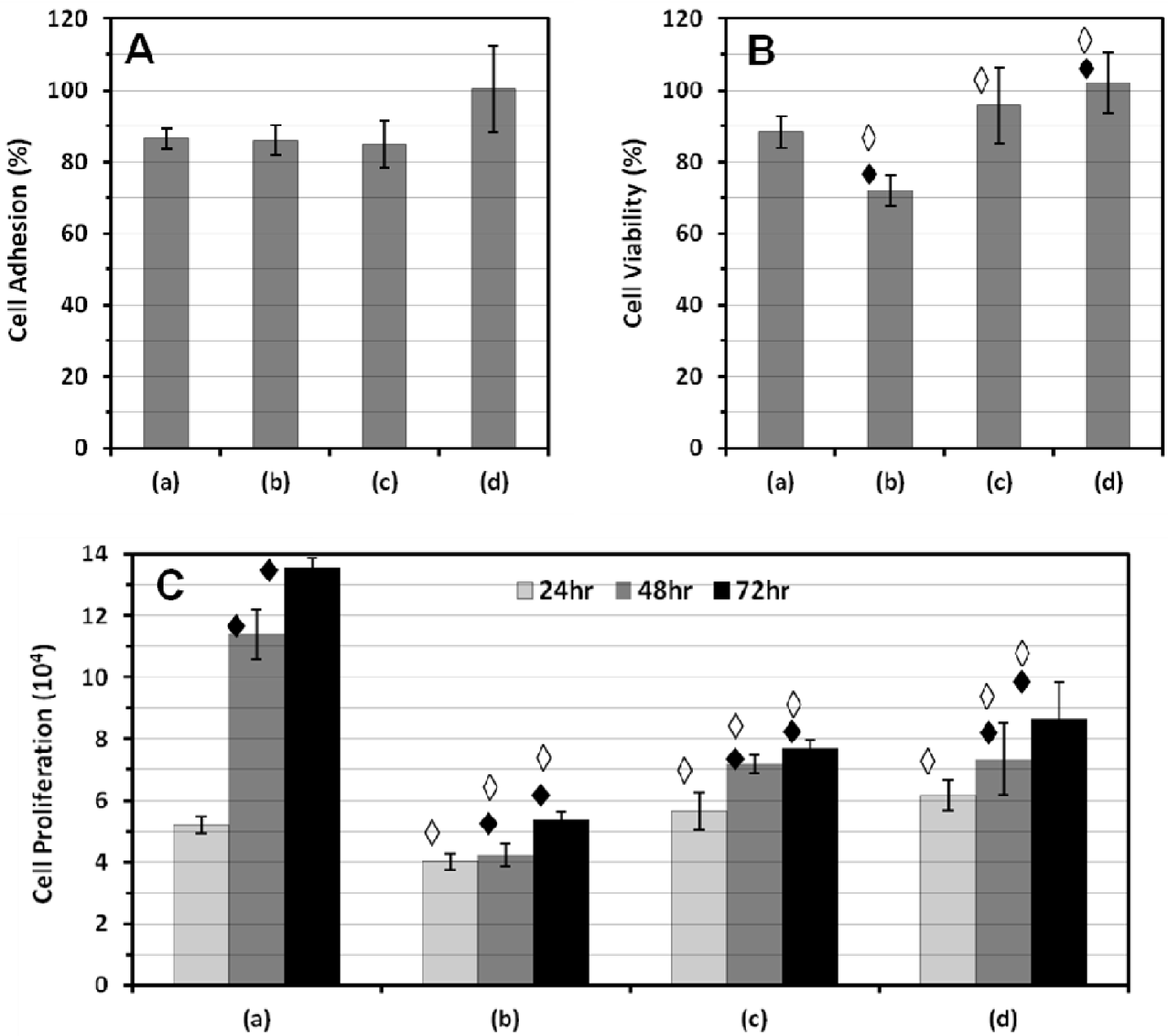
A
B
C
Cell Adhesion (%)
Cell Viability (%)
Cell Proliferation (10^4)
24hr
48hr
72hr
(a)
(b)
(c)
(d)

Figure 14